Accurate Analysis of Subharmonic Oscillations of V^2 and V^2I_C Controls Applied to Buck Converter

Jorge Cortés, *Student Member, IEEE*, Vladimir Šviković, *Student Member, IEEE*, Pedro Alou, *Member, IEEE*, Jesús A. Oliver, *Member, IEEE*, José A. Cobos, *Senior Member, IEEE*, and Rafael Wisniewski, *Member, IEEE*

***Abstract*— V^2I_c control provides very fast dynamic perfor- mance to the Buck converter both under load steps and under volt- age reference steps. However, the design of this control is complex since it is prone to subharmonic oscillations and several parameters affect the stability of the system. This paper derives and validates a very accurate modeling and stability analysis of a closed-loop V^2I_c control using the Floquet theory. This allows the derivation of sensitivity analysis to design a robust converter. The proposed methodology is validated on a 5-MHz Buck converter. The work is also extended to V^2 control using the same methodology, showing high accuracy and robustness. The paper also demonstrates, on the V^2 control, that even a low bandwidth-linear controller can affect the stability of a ripple-based control.**

***Index Terms*—Control of dc/dc converters, ripple based, robust- ness, V2, V2Ic.**

I. Introduction

V^2I_c CONTROL (see Fig. 1), proposed in [1], is a ripple- based controller that presents a very fast dynamic response under load steps and voltage reference steps. It is composed by a slow loop, where the output voltage is regulated with a linear controller, and a fast loop, where the error of the output voltage and the current through the output capacitor are added to the compensating ramp.

As the current through the output capacitor is the current through the inductor minus the output current, the control ex- hibits inherently a feedforward of the load current. Whenever the load changes, this variation is seen in the current through the output capacitor which changes instantaneously the control sig- nal and the duty cycle (see Fig. 2). This way, the control presents a very fast response under load perturbations. The error of the output voltage is also added in the fast loop and, consequently, a
step in the reference voltage causes an instantaneous reaction in the control signal. For this reason, V 2 Ic control is very appro- priate in applications where voltage reference tracking is also a requirement. A simplified version of V 2 Ic control, where the

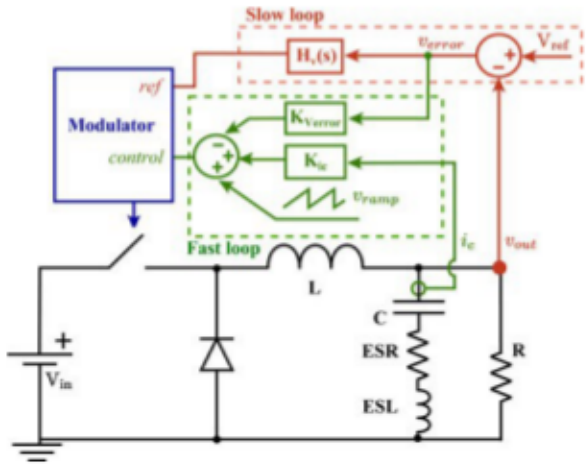

Fig. 1. Scheme of V^2I_c, a ripple-based controller.

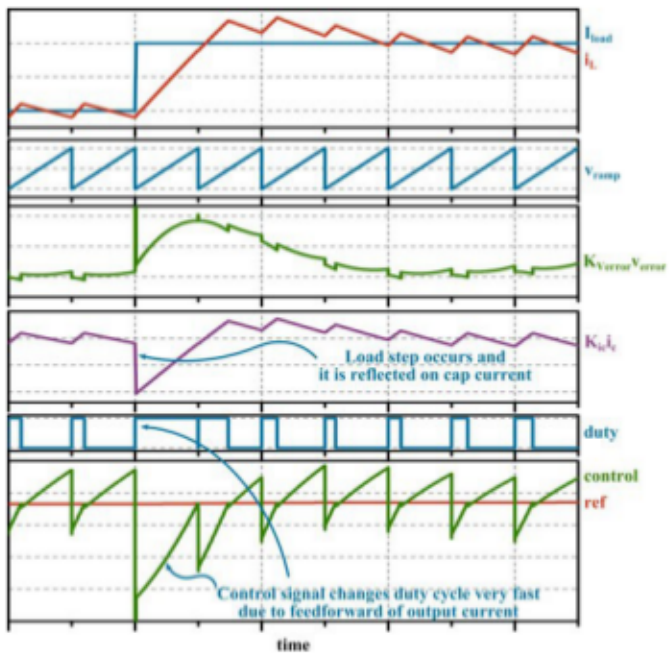

Fig. 2. Loading transient response of V^2I_c control.

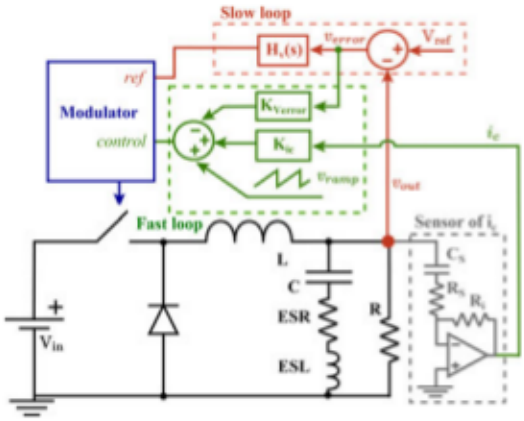

Fig. 3. $V^2 I_c$, with the capacitor current sensor.

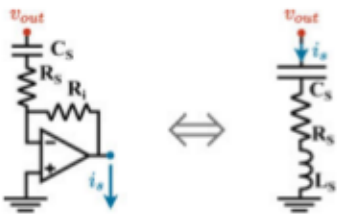

Fig. 4. Current sensor behaves like a *RLC* network.

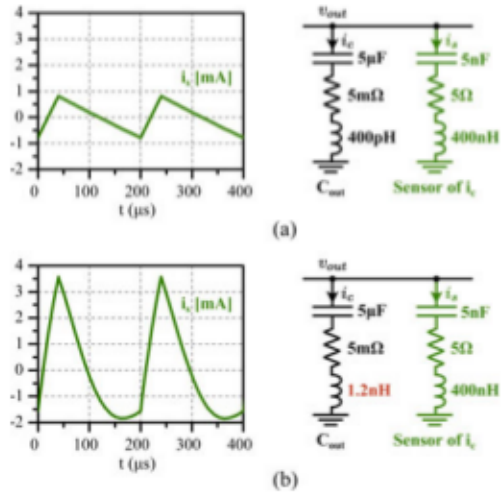

Fig. 5. (a) Current through the parallel network for a correct sensor design and (b) for a mismatch in the ESL of the output capacitor. (a) The sensor matches perfectly the impedance of the output capacitor. The measurement is correct. (b) The ESL of the output capacitor is larger than the one estimated. The measurement is distorted.

voltage reference is not included in the fast loop, is presented in [2] with constant on-time modulation and no artificial compensating ramp. The control techniques presented in [1] and [2] are, therefore, equivalent under load transients since the voltage reference acts as a constant offset under load perturbations.

The current through the output capacitor is sensed indirectly with a trans-impedance amplifier [3], [4] (see Fig. 3) in order not to change the impedance of the output capacitor. The current sensor is designed so that it behaves like an impedance proportional to the impedance of the output capacitor and, as a result, the measured current is proportional to the current through the output capacitor. When the switching frequency is very high, the output capacitor can be modeled as a complex capacitor with the parasitic elements equivalent series resistance (ESR) and equivalent series inductance (ESL). It is important to point out that the ESL does not only consider the parasitic inductance of the output capacitor but also the inductance added by the layout and, consequently, the range of variation of the ESL can be very large. For analysis purposes, the current sensor can be substituted by an equivalent *RLC* network with the same impedance as the current sensor (see Fig. 4). The correspondence between the components of the current sensor and the *RLC* equivalent network are detailed in [3], [4].

As explained, if the impedance (magnitude and phase) of the current sensor (*RLC* network) is proportional to the impedance of the output capacitor, then the current through the *RLC* network will mirror the current through the output capacitor with a certain gain. But a mismatch in the gain or phase will provoke a distorted measurement of the current as seen in the Fig. 5. The dynamic response under load disturbances is not significantly affected by the sensor mismatches. However, it may eventually induce subharmonic oscillations in the system because $V^2 I_c$ control uses that measurement as part of the control signal.

Since in real applications there might be tolerances in the value of the components and the control has to operate under these conditions, $V^2 I_c$ control needs to be robust against variations in the parasitic ESR and ESL of the output capacitor. The compensating ramp, the gain of the current sensor, and the gain of the error voltage of the fast loop are design parameters to keep stability over the desired operation range of the converter.

The goal of this paper is to accurately model a closed-loop $V^2 I_c$ control considering critical parameters like the parasitic ESR and ESL of the output capacitor and the tolerances in the current sensor (*RLC* network) and analyze its stability to carry out sensitivity analysis regarding tolerances of the system and the whole operating range to ensure a robust operation.

The paper is organized as follows: several techniques to model and analyze power converters are reviewed in Section II. Section III shows that a simplified modeling can lead to errors in the design of ripple-based controllers, and it is illustrated for a constant frequency V^2 peak control. Section IV derives and validates the proposed methodology based on the Floquet theory to analyze the $V^2 I_c$ control. Sections V and VI provide the experimental validation and the conclusions.

II. Review of Alternatives to Model, Analyze Stability, and Design Ripple-Based Controllers

In the scientific literature, there are several approaches to derive models of power converters that can predict subharmonic oscillations, mostly applied to common control techniques. Tan and Middlebrook [5] and Tang *et al.* [6] proposed a model for the peak current mode and the average current model control, respectively, both based on the modeling of the modulation stage. However, the derived transfer function of the modulator can only be applied to the triangular current and, consequently, it does not include the effect of the ripple of the voltage in

TABLE 1
ACCURACY OF THE DIFFERENT APPROXIMATIONS FOR THE EXPONENTIAL OF A MATRIX $A_1 T$ WITH AND WITHOUT CONSIDERING THE ESL

	$\mathbf{A_1}$ (symbolic)	$\mathbf{e^{A_1 T}}$	$\mathbf{I + A_1 T}$	$\mathbf{I + A_1 T + \frac{1}{2} A_1^2 T^2}$
without ESL	$\begin{pmatrix} \frac{-1}{C(R+ESR)} & \frac{R}{C(R+ESR)} \\ \frac{-R}{L(R+ESR)} & \frac{-R \cdot ESR}{L(R+ESR)} \end{pmatrix}$	$\begin{pmatrix} 0.94 & 0.04 \\ -1.93 & 0.95 \end{pmatrix}$	$\begin{pmatrix} 0.97 & 0.04 \\ -1.99 & 1 \end{pmatrix}$	$\begin{pmatrix} 0.93 & 0.04 \\ -1.96 & 0.95 \end{pmatrix}$
with ESL	$\begin{pmatrix} 0 & 0 & \frac{1}{C} \\ 0 & \frac{-R}{L} & \frac{R}{L} \\ \frac{-1}{ESL} & \frac{R}{ESL} & \frac{-(R+ESR)}{ESL} \end{pmatrix}$	$\begin{pmatrix} 0.94 & 0.04 & 0 \\ -1.92 & 0.95 & 0.004 \\ -2.53 & 0.92 & 0.004 \end{pmatrix}$	$\begin{pmatrix} 1 & 0 & 0.04 \\ 0 & -2 & 3 \\ -500 & 750 & -751.5 \end{pmatrix}$	$\begin{pmatrix} -9 & 15 & -15.01 \\ -750 & 1127.5 & -1130.2 \\ 187620 & -282560 & 283490 \end{pmatrix}$

the capacitor. Li and Lee [7] employed the describing function technique (DF) to model the V^2 constant on-time control as a unified system. These techniques provide a control-to-output and output impedance transfer function in symbolic form; based on these functions, an open-loop stability criterion, a study of the movement of poles and zeros [8], [9] and an equivalent circuit model [10], [11] can be derived. The DF technique achieves an excellent modeling of the V^2-controlled Buck converter and it is a very appropriate tool to understand the behavior of the system. DF is used to model a simplified version of $V^2 I_c$ control without an artificial compensating ramp in [2], deriving a design criterion for the constant on-time modulation. This proposed design guideline is also valid for the constant frequency modulation.

Although the design criterion is very useful, the modeling presented in [2] does not consider the mismatches in the current sensor which is crucial to predict sub-harmonic oscillations of the $V^2 I_c$ control. Also, it does not consider the ESL of the output capacitor because it is applied to a converter with a switching frequency in the order of hundreds of kHz where the ESL is not dominant. Consequently, this model is limited to predict the behavior of the converter under mismatches of the sensor or when the converter switches at a very high switching frequency and a more accurate analysis is needed to assure a robust operation.

In the 90s, the sub-harmonic oscillations started to be studied from the point of view of bifurcation phenomena. The sub-harmonic oscillation can be predicted by means of the Floquet theory that, for a T-periodic system, establishes whether a perturbation will grow or not over the period. The stability analysis can be carried out by either deriving the Jacobian matrix of the discrete model or by applying the Filippov's method to the piecewise-smooth model of the converter [12]. The evaluation of the stability is usually numerical but some papers have managed to derive design-oriented stability criteria [13], [14]. These stability criteria are obtained being open the slow loop and, therefore, the reference signal is constant rather than being controlled by a linear controller. Again, these design criteria are very useful but they must be carefully used since the applied simplifications limit their accuracy.

Unfortunately, when the slow loop is closed, the system usually tends to be more unstable. For example, an open-loop peak current-mode Buck converter without a compensating ramp becomes unstable from a duty cycle greater than 50% but when the voltage loop is closed, a sub-harmonic oscillation can appear for duty cycles less than 0.5 due to the rippled signal that appears at the output of the linear controller [6]. Although a sufficiently low bandwidth would deeply attenuate the ripple of the output voltage so that it seems that the ripple at the output of the linear controller could be neglected in practice, there is still a risk. Section III shows that a low bandwidth of $f_{sw}/40$ can critically affect the stability of a V^2 control. Therefore, an open-loop analysis results in a stability condition that does not represent the actual behavior of the closed-loop power converter. On the other hand, to derive a design-oriented closed-loop stability criterion based on Floquet theory may not be feasible in most cases. For the derivation of the symbolic discrete model, the differential equation $\dot{x} = Ax + Bu$ needs to be solved in time-domain and, for the common approach, A needs to be invertible. Unfortunately, the inclusion of the state variables of a controller with an integral action will make the matrix A non invertible and, thus, a symbolic discrete map cannot be derived. In [15], a closed-loop converter with a PI controller is modeled by considering only the proportional part of the controller, which is the dominant one at $f_{sw}/2$, since sub-harmonic oscillations are analyzed at this frequency. However, in ripple-based controls, a pure integral type-I controller is usually used so this approach is not sufficient.

Also, the inclusion of the ESL increases the complexity as it is illustrated in Table I. The derivation of design-oriented stability criteria using the discrete model relies on the simplification $e^{AT} \simeq I + AT$ or $e^{AT} \simeq I + AT + \frac{1}{2}A^2T^2$ which usually works remarkably well for power converters. But Table I shows for a 5 MHz Buck converter that, when the ESL is considered, the simplification is very inaccurate. The physical explanation behind this is that the current through the output capacitor, i_c, becomes a state variable with the inclusion of the ESL. But i_c is a very fast state variable when compared to the period due to the low value of the ESL and, consequently, the evolution of i_c cannot be approximated by a first or second order system. See for example Fig. 2 to notice that i_c can change abruptly while the dynamic response of the inductor current, i_L, can be approximated by a first or second order system. Therefore, a design-oriented closed-loop modeling and stability criteria of $V^2 I_c$ using the Jacobian matrix of the discrete model or Floquet theory is too complex and could be even not feasible.

As seen, there is a lot of effort in the academic literature to develop design-oriented models of ripple-based controllers. But in order to get useful ready-to-use design criteria, simplifications have to be made that could lead to inappropriate designs and, therefore, these models must be carefully used.

This paper proposes a very accurate numerical analysis of $V^2 I_c$ based on Floquet theory to ensure a robust operation. This necessary approach is complementary to a design-oriented modeling, such as the DF. The design-oriented modeling would define an initial design. Then, the proposed accurate stability

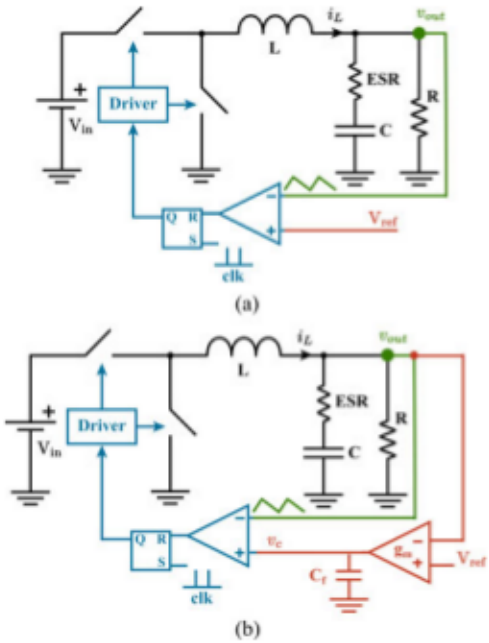

Fig. 6. Control scheme of a constant-frequency V^2 peak control. (a) V^2 with the slow loop opened. (b) V^2 with the slow loop closed for precise regulation of the output voltage.

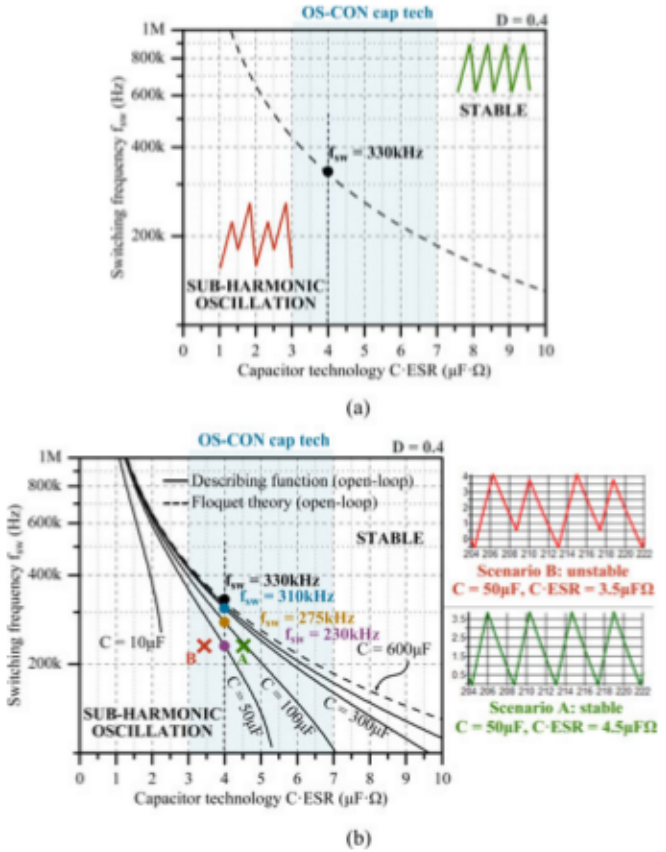

Fig. 7. Stability condition of constant frequency V^2 peak control and being the slow loop open using (a) DF and (b) Floquet theory. On the right of (b), the inductor current waveforms for an unstable case and a stable case are shown. (a) Stability condition from DF. (b) Comparison between DF and the Floquet theory.

analysis would carry out a sensitivity analysis being closed the slow loop and regarding critical parameters of the converter and mismatches in the current sensor. By using the sensitivity analysis, the initial design would be refined to a final robust design, if needed.

III. Need for Accurate Models

In Section IV, the proposed modeling and stability analysis of $V^2 I_c$ control is developed. However, before analyzing in detail the methodology and in order to motivate the work of the paper, this section illustrates on a constant frequency V^2 peak control, which is another ripple-based control, how a simplified modeling may lead to inappropriate designs and how an accurate analysis based on the Floquet theory can predict these mistakes.

The V^2 control [see Fig. 6(a)] is a ripple-based control that achieves a fast dynamic response under load steps while being very simple. The fast loop is composed by the output voltage and an optional ramp to increase the stability. Several modulation methods can be used [14] including constant on-time and constant frequency. The DF technique is proposed to analyze this control achieving very useful results by deriving symbolic transfer functions, symbolic stability criteria, and equivalent circuit models [10]. From them, ready-to-use design guidelines [8], [9] are derived to help to design these systems.

For the specific case of a constant frequency V^2 peak control with no compensating ramp, the stability criterion is found to be [9]

$$F_{sw} \geq \frac{1}{C \cdot \mathrm{ESR}} \cdot \left(\frac{1}{2} + \frac{D^2}{1-2D} \right) \qquad (1)$$

meaning that the stability of the converter is defined by its switching frequency, the capacitor technology given by its product $C \cdot \mathrm{ESR}$, and the duty cycle. This same stability criterion is also obtained from the simplified discrete model derived in [14]. Fig. 7(a) shows graphically the stability condition for a specific case with a duty cycle of 0.4. The dotted line represents the border between a stable system and the appearance of subharmonic oscillations and the light-blue shaded area indicates the area corresponding to the technology of OS–CON capacitors, which are commonly used for V^2 controls with no compensating ramp. For a capacitor with a product $4\,\mu\,\mathrm{F}\cdot\Omega$, the minimum switching frequency to maintain stability without a compensating ramp is 330 kHz according to the stability criterion.

Fig. 7(b) shows the stability condition of the converter using the accurate analysis proposed in this paper based on the Floquet theory. The dotted line represents the stability condition of Fig. 7(a) using DF. The parameters of the converter for the analysis using the Floquet theory are: $V_{\mathrm{in}} = 5\,\mathrm{V}$, $v_{\mathrm{out}} = 2\,\mathrm{V}$, $L = 1.3\,\mu\,\mathrm{H}$, and $R = 1$. The figure shows that the stability of the V^2 control depends not only on the capacitor technology, but also on the actual value of the capacitance of the output capacitor. For high capacitance values, the DF technique achieves very accurate results but it falls short for low capacitance values. For example, for $C = 50\,\mu\,\mathrm{F}$ and $C \cdot \mathrm{ESR} = 4\,\mu\,\mathrm{F}\,\Omega$, the minimum switching frequency is 230 kHz, that is 30% lower than the stability limit given by the DF technique. This stability

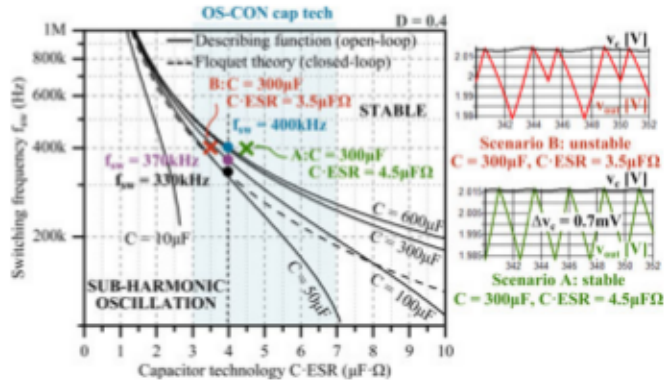

Fig. 8. Stability condition of constant frequency V^2 peak control and being the slow loop closed. On the right, the output voltage and the output of the linear controller for an unstable case and a stable case are shown.

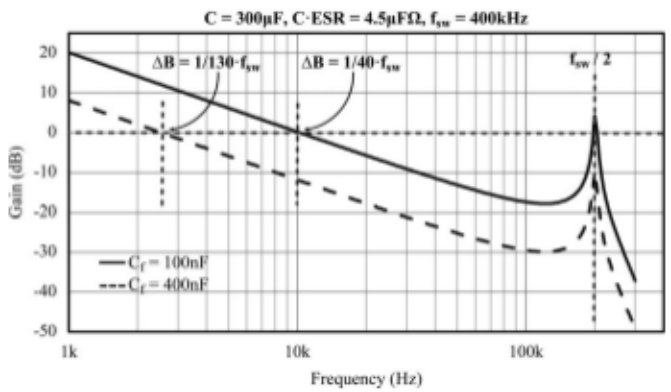

Fig. 9. Voltage loop gain of the slow loop for two different type-I controllers. Obtained from the Simplis simulations.

border is validated with the waveforms of Fig. 7(b), obtained from Simplis.

Now, in order to illustrate the effect of the slow loop, the Floquet theory is used to analyze the stability of the converter with the slow loop closed [see Fig. 6(b)]. Fig. 8 shows the border of stability for the same V^2 control but closing the slow loop with a type-I controller where the transconductance of the op-amp is $g_m = 6.4$ mA/V and $C_f = 100$ nF [see Fig. 6(b)]. The figure shows that the stable region is smaller, meaning that the subharmonic oscillations appear before in the closed-loop converter. Now, for high capacitance values, the stability condition derived from the DF technique for the open-loop converter is a risk. For $C = 600\,\mu$F and $C \cdot \text{ESR} = 4\,\mu\text{F}\Omega$, the minimum switching frequency is 440 kHz, compared to 330 kHz for the open-loop converter.

The waveforms of Fig. 8, obtained from the program Simplis, validate the stability analysis at a simulation level for a specific border of instability ($C = 300\,\mu$F, $C \cdot \text{ESR} = 4\,\mu$F, $f_{sw} = 400$ kHz, and $C_f = 100$ nF). Notice that the ripple of the output of the linear controller, v_c, is highly attenuated (the peak-to-peak voltage is 0.7 mV) due to the low bandwidth but still affects the stability of the converter. Fig. 9 shows that the bandwidth of the voltage loop gain of the slow loop at the border of this instability is 10 kHz $= f_{sw}/40$ and that the converter can be stabilized by further decreasing the bandwidth by increasing

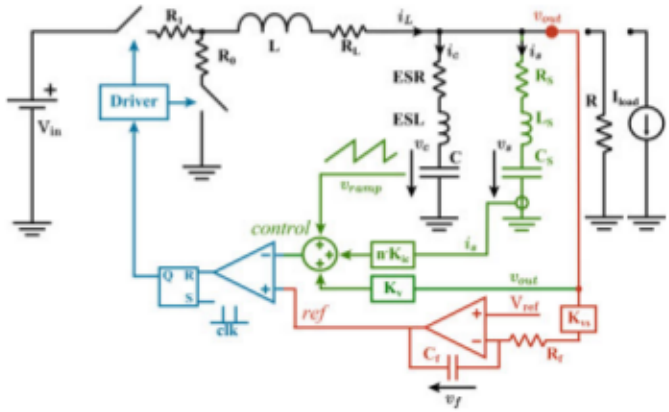

Fig. 10. Scheme of a V^2I_c-controlled Buck converter with constant frequency modulation.

C_f. Fig. 9 shows that, when the slow loop has a bandwidth of $f_{sw}/130$, the peak of the voltage loop gain at half of the switching frequency does not return to 0 dB and, consequently, the converter is stable.

This study shows that, for more reliable results, the stability of the converter needs to be addressed with the slow loop closed rather than simplifying it in open-loop form because even a low bandwidth of $f_{sw}/40$ can affect the stability.

This study also motivates the need of the proposed approach to evaluate the stability of ripple-based controllers in closed-loop and with very precise techniques as a complement to design-oriented models.

IV. Proposed Approach to Analyze V^2I_c Control

This section explains the modeling of the V^2I_c control based on discrete modeling and the stability analysis based on the Floquet theory. It is divided in three subsections where the derivation of the discrete model, the stability analysis and the sensitivity analysis are explained and validated with simulations.

The assumption of the modeling is that the converter can be described by a piecewise-smooth state-space model with two states: on (state 1) and off (state 0). Therefore, the model does not include delays, saturations, or dead-times.

A. Discrete Modeling of V^2I_c

This section explains the derivation of the discrete modeling of the V^2I_c control [1] (see Fig. 10). Notice that, in Fig. 10, the fast loop uses the output voltage with a gain K_v, instead of the error of the output voltage with a gain $K_{V\text{error}}$ as in Fig. 3. This is because, with the implementation of the linear controller with the operational amplifier, the reference voltage is already summed in the reference signal as it is $V_{\text{ref}} - v_f$. Also notice that in Fig. 10, the current sensor has been substituted by the equivalent *RLC* network. The pulse width modulation is made using a latch RS and a clock signal to provide constant switching frequency.The figure shows the model of the V^2I_c control with all the considered parasitic elements. The on-resistance of the switches R_1 and R_0, the resistance of the inductor, R_L, the ESR,

and the ESL of the output capacitor are the parasitic elements of the power stage. The compensating ramp, $v_{\rm ramp}$ is modeled over a period T as $v_{\rm ramp}(t) = m_{\rm ramp} \cdot t + H$, where $m_{\rm ramp}$ is the slope of the ramp and H is the offset voltage. The peak-to-peak amplitude of the ramp is $V_{pp} = m_{\rm ramp} \cdot T$. The linear regulator, $H_v(s)$ in Fig. 3, is implemented as a type-I controller with resistance R_f and capacitor C_f. The gain of the output voltage inside the fast loop is K_v and the gain of the output voltage inside the slow loop is K_{vs}, which takes into account an optional gain in the measurement of the output voltage.

1) Measurement of the Current Through the Output Capacitor: The current through the output capacitor is measured by adding a parallel *RLC* network [3], [4]. The actual implementation is done by means of a trans-impedance amplifier but, for the analysis of the control, it is sufficient to consider only the equivalent parallel *RLC* network. For a correct measurement of the current, the impedance of the parallel network must be proportional to the impedance of the output capacitor, $Z_{C_{\rm out}} = n \cdot Z_{RLC}$, where n is the gain of the current sensor

$$C_s = \frac{C}{n}; \quad R_s = n \cdot \text{ESR}; \quad L_s = n \cdot \text{ESL}. \tag{2}$$

When these conditions are fulfilled, the current through the parallel network is $1/n$ times the current through the output capacitor

$$i_s = i_c \cdot \frac{1}{n}. \tag{3}$$

The measurement of the output capacitor current is, then, weighted with a gain K_{ic}.

$V^2 I_c$ control is sensitive to variations of the ESL of the output capacitor. A mismatch in the ESL will provoke a distorted measurement of the current i_c and, since it is a ripple-based control that uses i_c as a triangular control signal, it may eventually induce subharmonic oscillations in the system.

2) Piece-Wise Smooth Model of the System: The state variables, x, of the system are the voltage in the output capacitance, v_c, the voltage in the capacitance of the parallel network, v_s, the current through the inductor, i_L, the current through the output capacitor, i_c, the current through the parallel network, i_s, and the voltage in the capacitor of the regulator, v_f

$$x(t) = \big(v_c(t), v_s(t), i_L(t), i_c(t), i_s(t), v_f(t)\big)^T. \tag{4}$$

The input variables, u, are the input voltage, $V_{\rm in}$, the reference voltage, $V_{\rm ref}$, and the added current demanded by the load, $I_{\rm load}$, which is used to perform load transients

$$u = (V_{\rm in}, V_{\rm ref}, I_{\rm load})^T. \tag{5}$$

The general form of a piece-wise smooth model of a converter with two states, like the Buck converter with $V^2 I_c$ control, is of the form of

$$\frac{dx(t)}{dt} = \begin{cases} A_0 x(t) + B_0 u, & \text{if state 0} \\ A_1 x(t) + B_1 u, & \text{if state 1} \end{cases} \tag{6}$$

where the state 1 is when the high-side MOSFET of the Buck converter is conducting and the state 0 is when the low-side MOSFET is conducting. The matrices and vector of the piecewise-smooth model of the Buck converter with $V^2 I_c$ control are shown in Appendix A.

The switching hyper-surface that takes into account the switching from state 1 to state 0 is the intersection of the control signal with the reference signal (the input signals of the comparator in Fig. 10)

$$h_{10}(x,t) = v_{\rm control}(t) - v_{\rm reference}(t). \tag{7}$$

The control signal, $v_{\rm control}$, presents the fast rippled signals. It is composed by the measurement of the current through the output capacitor weighted by a factor, $n \cdot K_{ic} \cdot i_c$, by the weighted output voltage, $K_v \cdot v_{\rm out}$, and by a compensating ramp, $v_{\rm ramp}$

$$v_{\rm control}(t) = v_{\rm ramp}(t) + n \cdot K_{ic} \cdot i_c(t) + K_v \cdot v_{\rm out}(t). \tag{8}$$

The reference signal, $v_{\rm reference}$, presents the slow regulated signal. It is composed by the reference voltage, $V_{\rm ref}$, and voltage in the capacitor of the linear controller, v_f

$$v_{\rm reference}(t) = V_{\rm ref} - v_f(t). \tag{9}$$

Combining (4), (5), (7), (8), and (9), the switching condition to go from state 1 to state 0 is

$$h_{10}(x,t) = Kx(t) + Gu + m_{\rm ramp} t + H = 0 \tag{10}$$

where

$$K = (0, 0, K_v R, -K_v R, K_{ic} n - K_v R, -1) \tag{11}$$

$$G = (0 - 1 K_v R). \tag{12}$$

Due to the integral action of the closed-loop control, the matrices A_0 and A_1 are noninvertible. Then, the solution of the differential equation $dx(t)/dt = Ax(t) + Bu$, needed for the derivation of the discrete model, cannot be directly solved, and rather, another approach is needed.

The augmented state-vector [16] provides an elegant method to solve the problem by creating a new variable vector, y, which is composed by the state variables (4) and the input variables (5)

$$y(t) = \big(v_c(t), v_s(t), i_L(t), i_c(t), i_s(t), v_f(t), V_{\rm in}, V_{\rm ref}, I_{\rm load}\big)^T. \tag{13}$$

In this way, the system can be defined as

$$\frac{dy(t)}{dt} = \begin{cases} \hat{A}_0 y(t), & \text{if state 0} \\ \hat{A}_1 y(t), & \text{if state 1} \end{cases} \tag{14}$$

where

$$\hat{A}_0 = \begin{pmatrix} A_0 & B_0 \\ 0 & 0 \end{pmatrix}; \qquad \hat{A}_1 = \begin{pmatrix} A_1 & B_1 \\ 0 & 0 \end{pmatrix}. \tag{15}$$

The switching hyper-surface that takes into account the switching from state 1 to state 0 is

$$h_{10}(y,t) = \hat{K} y(t) + m_{\rm ramp} t + H \tag{16}$$

where

$$\hat{K} = (K, G) \tag{17}$$

3) Discrete Model of the System: The discrete model of the system is a function or collection of functions that relate the state variables at the beginning of a period with the state variables at the end of that period.

Let T be the switching period of the control and the sample period of the discrete model. Let the initial state, y_k, be the value of the variables of the vector $y(t)$ at the beginning of the period and let the final state, y_{k+1}, be the value of the variables of the vector y at the end of the period. Let d be the duty cycle, where $t = dT$ is the time at which the converter changes to state 0.

1) From $t = 0$ to $t = dT$, the converter is in state 1 and the differential equation governing the system is

$$\frac{dy(t)}{dt} = \hat{A}_1 y(t). \tag{18}$$

The time-domain solution of (18) is

$$y(t) = e^{\hat{A}_1 t} \cdot y_k \tag{19}$$

2) At $t = dT$, the system switches from state 1 to state 0. Equation (16) represents the switching condition and can be used to derive a relation between the duty cycle and the initial state

$$h_{10}\big(y(dT), dT\big) = \hat{K} y(dT) + m_{\text{ramp}} dT + H = 0 \tag{20}$$

Equation (19) evaluated at $t = dT$ is

$$y(dT) = e^{\hat{A}_1 dT} \cdot y_k \tag{21}$$

Substituting (21) in (20) yields the relation between the duty cycle and the initial state

$$g(y_k, d) = 0 \tag{22}$$

where

$$g(y_k, d) = \hat{K} \cdot e^{\hat{A}_1 dT} y_k + m_{\text{ramp}} dT + H = 0. \tag{23}$$

3) From $t = dT$ to $t = T$, the converter is in state 0 and the differential equation governing the system is

$$\frac{dy(t)}{dt} = \hat{A}_0 y(t). \tag{24}$$

The time-domain solution of (24) is

$$y(t) = e^{\hat{A}_0 (t - dT)} \cdot y(dT). \tag{25}$$

Substituting (21) in (25) yields the time-domain solution of state 0 as a function of the duty cycle and the initial state

$$y(t) = e^{\hat{A}_0 (t - dT)} e^{\hat{A}_1 dT} y_k \tag{26}$$

Equation (26) evaluated at $t = T$ yields the relation between the final state and the initial state and the duty cycle

$$y_{k+1} = f(y_k, d) \tag{27}$$

where

$$y_{k+1} = e^{\hat{A}_0 (1-d)T} \cdot e^{\hat{A}_1 dT} \cdot y_k. \tag{28}$$

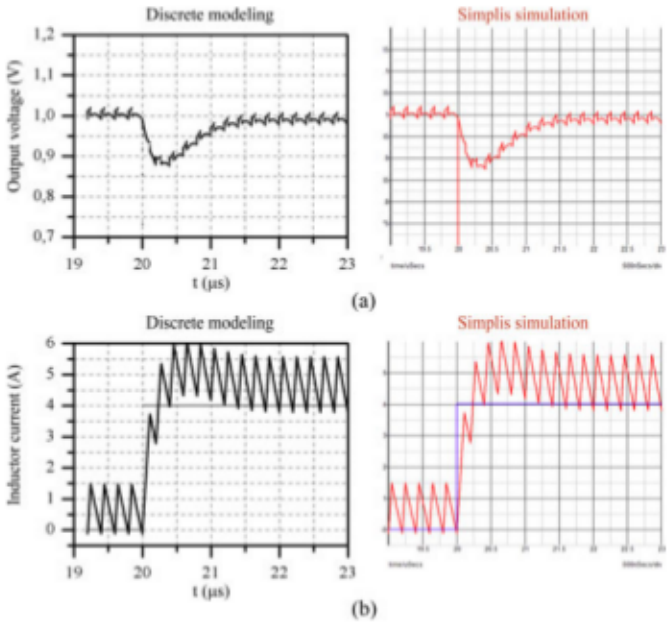

Fig. 11. Comparison between the discrete model (left) and simulation results (right) under a load step 0 A → 4 A. (a) Output voltage. (b) Inductor current.

Equations (22) and (27) form the large-signal closed-loop implicit discrete model of the converter

$$y_{k+1} = f(y_k, d); \qquad g(y_k, d) = 0. \tag{29}$$

Normally, this model would be explicit, where the duty cycle can be obtained as an explicit function of the initial state[1], but this is achieved by simplifying the exponential term of (23) by its first or second Taylor expansions.[2] However, when the ESL of the output capacitor is included in the model, this simplification is not valid (refer to Table I) and therefore the function that relates the initial state and the duty cycle is implicit.

Notice that the discrete model is not a discrete transfer function $G(z)$. The derived discrete model is nonlinear and presents no simplifications. Furthermore, the state variables at any point can be obtained from the model using equations (19) and (26). For a fast computation time, (29) can be used to show only the state variables at the beginning of each period, whereas equations (19), (22), and (26), which define the time-domain evolution of the state variables, can be used for a detailed simulation that includes the ripple of the signals. Unless otherwise specified, this paper uses this last method for the discrete modeling results.

Figs. 11 and 12 show a comparison between the discrete model derived including the ripple and simulation results from the commercial program Simplis. The parameters of the converter are: $V_{\text{in}} = 4.5\,\text{V}$, $v_{\text{out}} = 1\,\text{V}$, $I_{\text{load}} = 0\,\text{A}$, $R = 1.8\,\Omega$, $L = 100\,\text{nH}$, $R_L = 10\,\text{m}\Omega$, $R_1 = R_0 = 50\,\text{m}\Omega$, $C = 5\,\mu\text{F}$, $\text{ESR} = 5\,\text{m}\Omega$, $\text{ESL} = 400\,\text{pH}$, $K_i = 1/(R_f C_f) = 3.7 \cdot 10^5 \Omega^{-1}\text{F}^{-1}$, $K_v = 1$, $K_{vs} = 1$, $K_{ic} = 0.12$, $V_{pp} = m_{\text{ramp}} T =$

[1] An explicit function that relates the duty cycle and the initial state is of the form: $d = \varphi(y_k)$

[2] The first and second Taylor expansion of an exponential matrix are: $e^{\hat{A}_1 dT} \simeq I + \hat{A}_1 dT \simeq I + \hat{A}_1 dT + \frac{1}{2}\hat{A}_1^2 d^2 T^2$

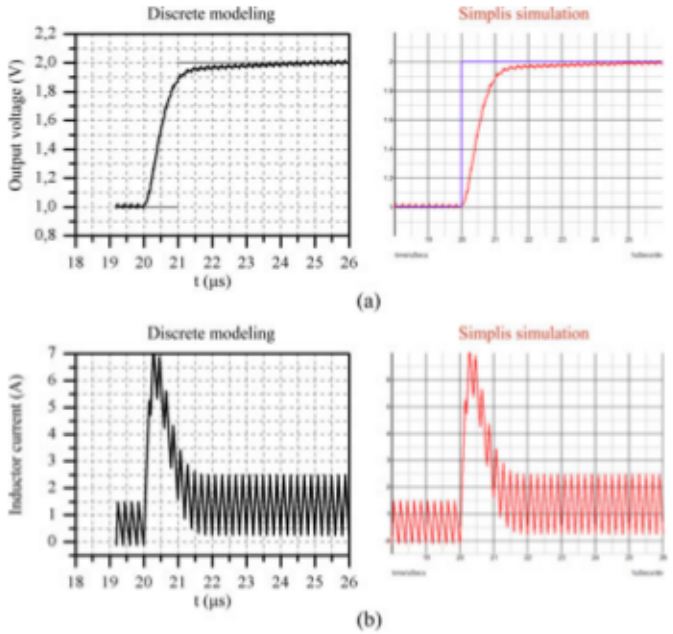

Fig. 12. Comparison between the discrete model (left) and simulation results (right) under a voltage reference step 1 V → 2 V. (a) Output voltage. (b) Inductor current.

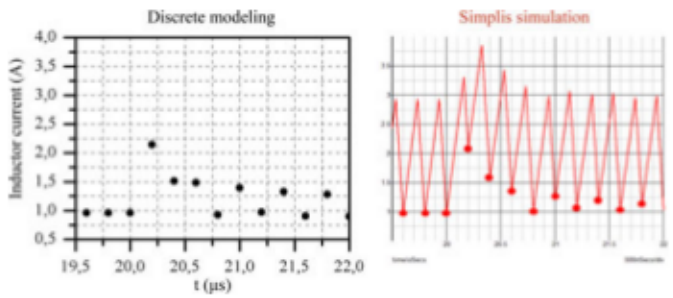

Fig. 13. Comparison between the discrete model (left) and simulation results (right) under a subharmonic oscillation. Only the values of the inductor current at the beginning of each period are shown in the discrete model. The values of the inductor current at the beginning of each period have been highlighted in the simulation results.

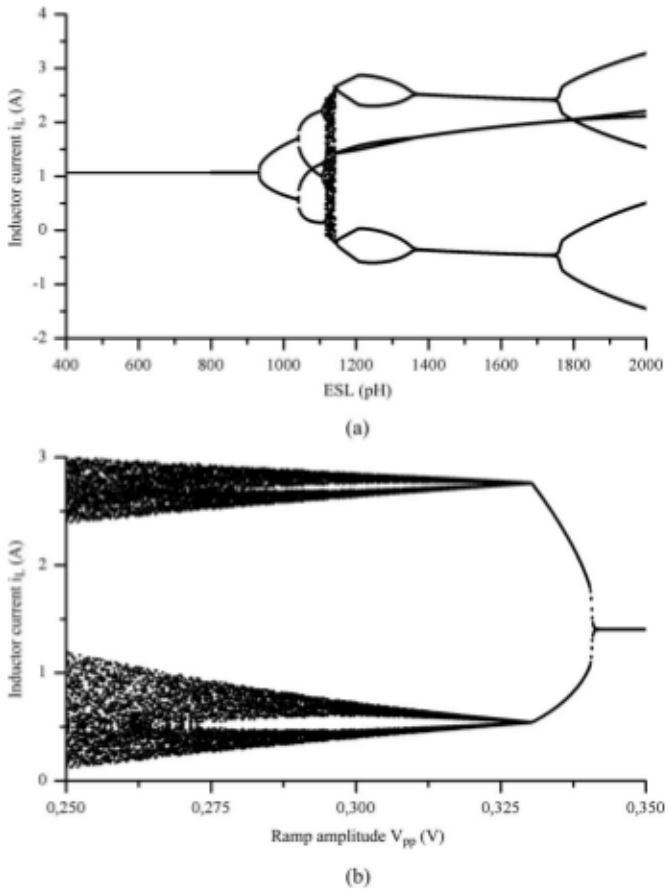

Fig. 14. Bifurcation diagrams for sensitivity analysis varying the ESL of the output capacitor and the compensating ramp. Sensor designed for ESL = 400 pH. (a) Varying ESL. Subharmonic oscillations when ESL > 930 pH. (b) Varying amplitude of compensating ramp, V_{pp}. Sub-harmonic oscillations when $V_{pp} < 0.34$V.

0.9V, $H = 0$, V. The current sensor is designed with a gain of $n = 1000$: $C_s = C/n = 5$ nF, $R_s = n\text{ESR} = 5\Omega$, $L_s = n\text{ESL} = 400$ nH. The dynamic behavior and the ripple of the signals greatly agree, validating the goodness of the model.

Fig. 13 verifies that the subharmonic oscillations appear at the same time both in the discrete modeling and the simulation program. The ESL is changed to 930 pH, causing a mismatch in the *RLC* network that distorts the measurement of the current through the output capacitor. This causes a subharmonic oscillation from $v_{\text{out}} = 3.1$ V in both cases. The figure shows that, at $v_{\text{out}} = 3$ V, the converter is stable. Then, at $t = 20\,\mu$ s, the voltage reference changes from 3 to 3.1 V and a subharmonic oscillation occurs.

Fig. 14 shows a bifurcation diagram for sensitivity analysis that can be used to graphically represent the subharmonic oscillations of the converter: as a parameter of the power converter is swept, the value of one state variable at the beginning of each period is plotted a large number of times when the steady state has been reached. Notice that the instability, called in power electronics subharmonic oscillation, is in control theory a double-period bifurcation where the system is unable to achieve periodicity in a period T and, rather, the steady-state orbit is $2T$-periodic. Therefore, the system is within a subharmonic oscillation if two or more alternating values are seen in steady state when a state variable is sampled every period T. When the system becomes more and more unstable, more alternating values appear until it enters into a chaotic behavior where the system erratically oscillates.

Fig. 14(a) shows the bifurcation diagram varying the ESL of the output capacitor with the sensor designed for an ESL of 400 pH and $v_{\text{out}} = 3.1$ V. It indicates that the subharmonic oscillations will occur for ESL greater than 930 pH.

Fig. 14(b) shows the bifurcation diagram varying the compensating ramp with ESL = 400 pH (no mismatch) and $v_{\text{out}} = 3.3$ V. It indicates that subharmonic oscillations appear when the amplitude of the ramp is lower than 0.34 V.

B. *Stability Analysis of $V^2 I_c$*

This section explains the stability analysis of the $V^2 I_c$ control using the Floquet theory. The Filippov's method [12], [17] is

employed to find out the monodromy matrix. The Floquet theory and the Filippov's method are briefly explained in Appendix B.

1) Values of the State Variables: The Filippov's method requires the value of the state variables at the switching events. This value can be retrieved from a simulation program but the derived discrete model can be used to directly obtain the periodic operating point of the system. From (29), the constraint $y_{k+1} = y_k$ is applied. Then, the values of the state variables in steady state at the beginning of the period are found out numerically. Equation (21) allows then to find out the values of the state variables at the switching events.

For the $V^2 I_c$ control, the switching event at the end of the period is forced, so it does not have to be considered. The other switching event happens at $t = dT$, so the following variables need to be obtained:

$$x(dT) = \left(v_c(dT), v_s(dT), i_L(dT), i_c(dT), i_s(dT), v_f(dT)\right)^T. \tag{30}$$

2) Filippov's Method: Equation (47) shows the expression of the monodromy matrix using the Filippov's method. The saltation matrix corresponding to the first switching, which occurs at $t = dT$ is

$$S_1(dT) = I + \frac{(f_{dT+} - f_{dT-})n^T}{n^T f_{dT-} + \frac{\partial h}{\partial t}(dT, x(dT))} \tag{31}$$

where $f_{dT+} = A_0 x(dT) + B_0 u$, $f_{dT-} = A_1 x(dT) + B_1 u$, $n = K$ and $\partial h/\partial t(dT, x((dT)) = m_{\text{ramp}}$.

The monodromy matrix is

$$\phi_{\text{cycle}} = e^{A_0(1-d)T} \cdot S_1(dT) \cdot e^{A_1 dT}. \tag{32}$$

If all the eigenvalues, called the Floquet multipliers, are inside the open unit disk, the system is locally asymptotically stable.

Fig. 15 shows a comparison between the bifurcation diagrams of Fig. 14 and the stability analysis, showing a complete agreement that validates the method at simulation level. When varying the ESL of the output capacitor or the compensating ramp, the system becomes unstable at the same moment that one eigenvalue goes out of the open unit disk.

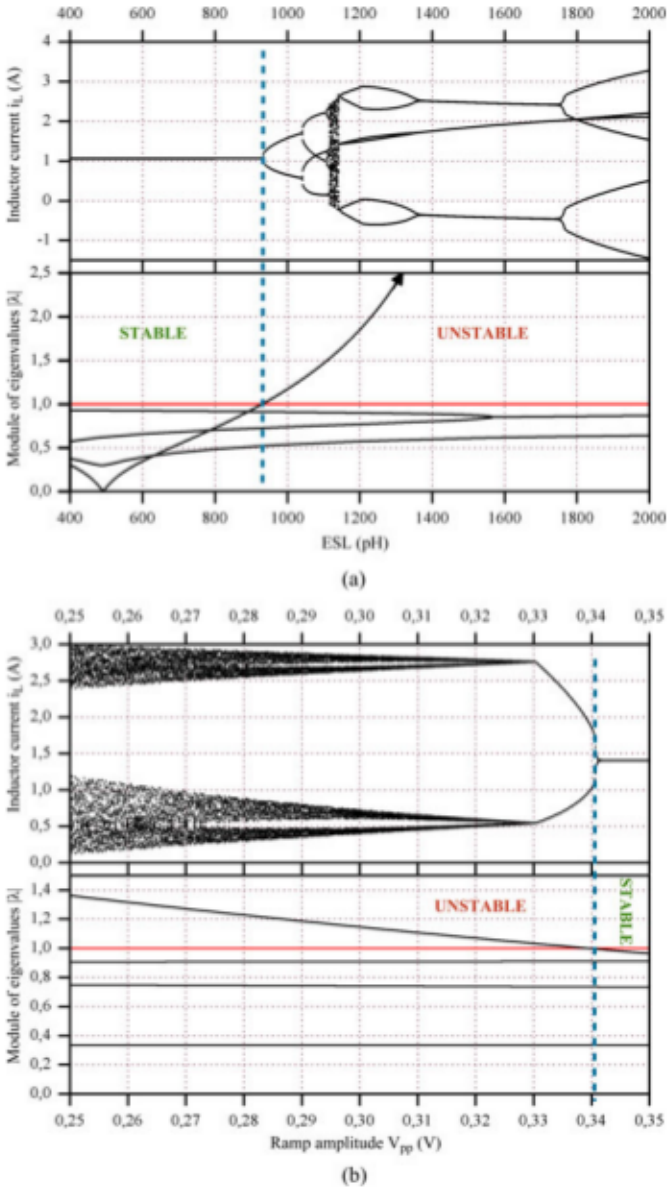

Fig. 15. Comparison of the bifurcation diagrams and the stability analysis. Upper part of (a) and (b): inductor current sampled every T seconds. Lower part of (a) and (b): module of the eigenvalues. (a) Varying ESL. Sensor designed for ESL $= 400$ pH. (b) Varying amplitude of compensating ramp.

C. Sensitivity Analysis of $V^2 I_c$

The combination of discrete modeling and the Floquet theory allows the derivation of powerful tools: as critical parameters of the power converter are varied, the required values of the state variables are retrieved from the discrete modeling, and the Filippov's method is employed to compute the Floquet multipliers and establish stable region diagrams. In this section, the methodology is applied to a Buck converter with $V^2 I_c$ control.

Several parameters are to be considered to perform a full sensitivity analysis of the $V^2 I_c$ control. Subharmonic oscillations and stability issues depend on the range of the duty cycle operation, gain of the capacitor current loop, slope of the compensating ramp, variation of the ESL of the output capacitor, and mismatches of the current sensor. The proposed sensitivity analysis based on the Floquet theory accounts for all these parameters. The parameters of the converter are the same as in Section IV. Fig. 16 shows the sensitivity analysis by means of stable region diagrams where the horizontal axis is the duty cycle and the vertical axis is the amplitude of the compensating ramp. The lines separate the stable region from the unstable region for different cases of ESL. From the analysis, designs can be made that are robust under tolerances against variation of the ESL of the output capacitor.

Fig. 16(a) shows the stable region when the sensor is perfectly-matched. It shows that, for duty cycles lower than 0.45, no compensating ramp is needed. For a case of $d = 0.7$, at least a ramp of 0.3 V of amplitude is needed. The relation between the duty cycle and the ramp is linear as in peak current mode control and it seems that a symbolic stability criteria could be derived that accounts for the perfectly-matched sensor.

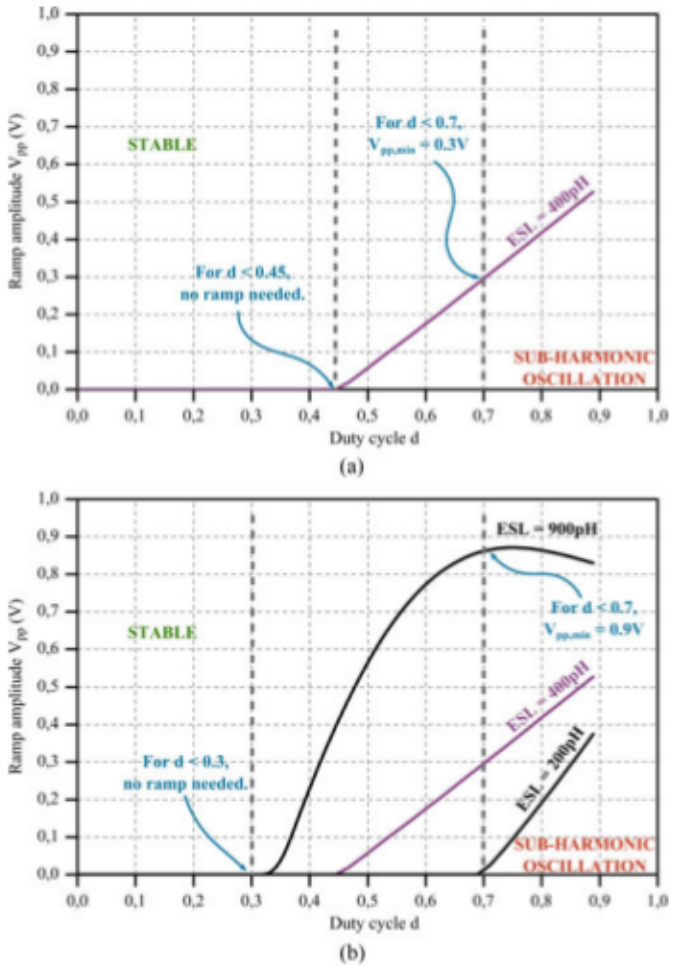

Fig. 16. Sensitivity analysis of $V^2 I_c$. It shows the required compensating ramp for different duty cycles and ESL of the output capacitor. The stable regions are the upper area of the curves. Sensor designed for ESL = 400 pH.

But when the ESL varies from the estimated value, the stability criteria greatly changes. Fig. 16(b) shows the stable regions for two extreme cases: an ESL of 900 and 200 pH. When the ESL is 900 pH and the sensor is designed for 400 pH, the relation between the duty cycle and the ramp becomes nonlinear and the converter is more unstable. For that case, no compensating ramp would be needed for duty cycles lower than 0.3 and, now, at a duty cycle of 0.7, the minimum ramp would be 0.9 V, which is a great increase compared to the ramp of 0.3 V for the case of a perfectly-matched sensor. When the ESL is 200 pH, the converter becomes more stable.

This analysis shows that a stability analysis without considering the ESL of the output capacitor or the parallel *RLC* network would not be sufficient for an accurate analysis.

The modeling and the stability analysis derived allow the design of robust converters with $V^2 I_c$ control. For example, if for this selected system, the duty cycle ranges between 20% and 70% and the nominal ESL is 400 pH but the designer wants to set a safe band of tolerance so that the ESL can vary between 200 and 900 pH without instability, then the minimum ramp of the control needs to be 0.9 V.

V. Experimental Validation

This section documents the validation of the discrete modeling and stability analysis of the $V^2 I_c$ control. The experimental prototype is designed according to the sensitivity analysis of Section IV-C.

The parameters of the converter are: $V_{\text{in}} = 4.5\,\text{V}$, $v_{\text{out}} = 1\,\text{V}$, $I_{\text{load}} = 0\,\text{A}$, $R = 1.8\,\Omega$, $L = 100\,\text{nH}$, $R_L = 10\,\text{m}\Omega$, $R_1 = R_0 = 40\,\text{m}\Omega$, $C = 4\,\mu\text{F}$, $\text{ESR} = 5\,\text{m}\Omega$, $\text{ESL} = 1.2\,\text{nH}$, $R_f = 1\,\text{k}\Omega$, $C_f = 2.4\,\text{nF}$, $K_v = 1$, $K_{vs} = 1$, $K_{ic} = 0.245$, $V_{pp} = m_{\text{ramp}} T = 1.3\,\text{V}$, $H = 0\,\text{V}$. The current sensor is designed with a gain of $n = 1000$: $C_s = C/n = 4\,\text{nF}$, $R_s = n\text{ESR} = 5\,\Omega$, $L_s = n\text{ESL} = 1.2\,\mu\text{H}$.

The comparison of the discrete map and the experimental results is shown under a negative voltage reference step. This section is divided in two parts: validation of the discrete modeling and validation of the stability analysis.

A. Validation of Discrete Modeling

The discrete modeling of the system is validated by comparing the dynamic behavior of the modeling under a voltage reference step with the experimental behavior measured in the prototype.

The system is subjected to a negative voltage reference step of 2V → 1see (see Fig. 17).

The dynamic behavior of the discrete model and thebrk experimental prototype greatly agree.

B. Validation of Analysis of Local Stability

The previous parameters remain the same except the ramp, which is set to an amplitude of 0.37 V in order to provoke an instability.

The Floquet theory predicts that the system becomes unstable from an output voltage of 3.1 V (see Fig. 18): for $v_{\text{out}} = 3\,\text{V}$, all the Floquet multipliers remain inside the unit circle, but one of them is on the border at -0.9654. When the output voltage is increased to 3.1 V, that multiplier is -1.064, and thus, gets out of the unit circle. The Floquet theory states, then, that the converter is unstable at $v_{\text{out}} = 3.1\,\text{V}$.

This prediction is validated experimentally (see Fig. 19). The converter becomes unstable at the very same point predicted by the analysis, resulting in a very precise method to predict instabilities. Specifically, in the experimental validation, the voltage reference is increased from 3 to 3.1 V. Notice that, in the time scale of Fig. 19, the output voltage still does not fully reach 3.1 V. The reason to use this small time scale is to highlight the beginning of the instability. The experimental validation shows that the system is in the very limit of the stability since the subharmonic oscillations appear when the output voltage is slightly increased over 3 V. This is accurately predicted by the proposed analysis ($\lambda = -0.9654$ for $v_{\text{out}} = 3\,\text{V}$).

VI. Conclusion

Ripple-based controls like V^2 and $V^2 I_c$ can achieve outstanding dynamic performance but their design is complicated and accurate modeling and deep stability analysis must be applied to

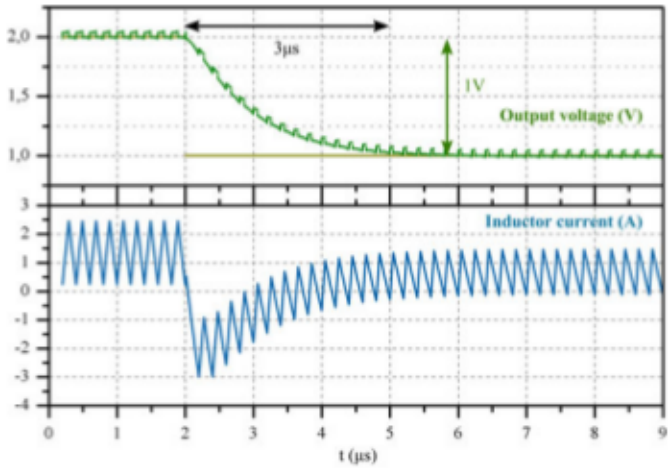

(a)

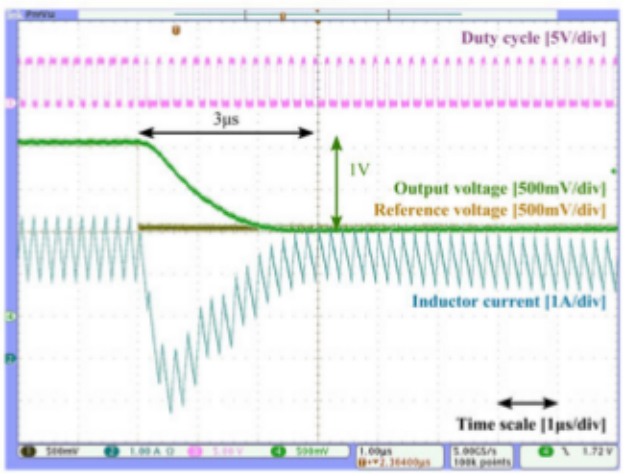

(b)

Fig. 17. Experimental validation of discrete modeling under a voltage reference step 2 V → 1 V. (a) Discrete modeling. (b) Experimental prototype.

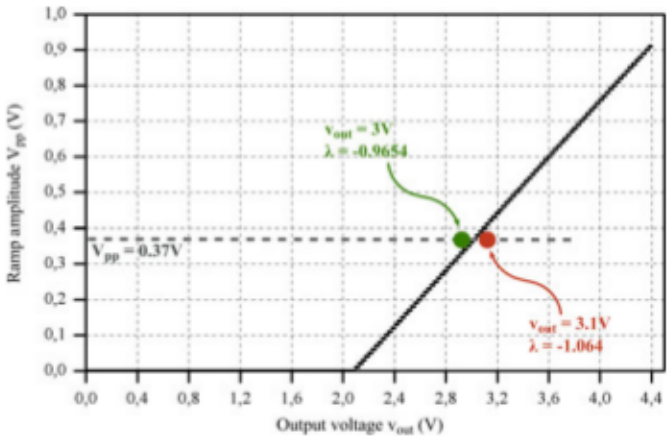

Fig. 18. Stable region diagram varying compensating ramp and output voltage. The eigenvalues and the output voltages at the border of stability are shown for a ramp with an amplitude voltage of $V_{pp} = 0.37\,\mathrm{V}$.

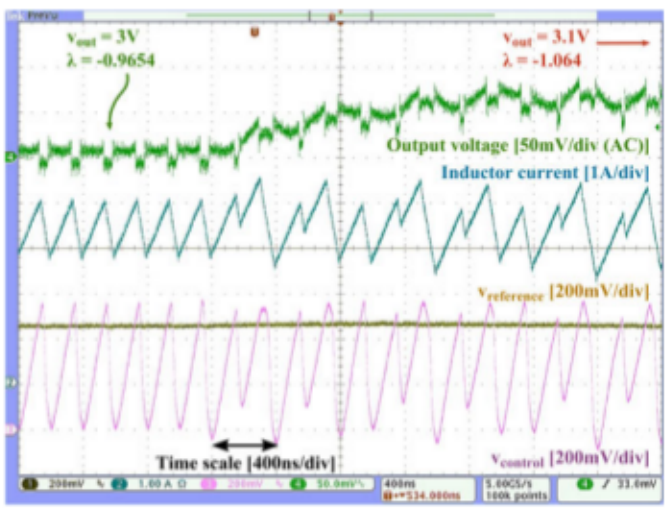

Fig. 19. Experimental validation of the stability analysis of Fig. 18. The converter becomes unstable under a voltage reference step 3 V → 3.1 V.

assure stability and robustness under the whole operation range of the converter as well as regarding the tolerances of the system. The paper proposes to use a very accurate numerical modeling based on discrete modeling and stability analysis based on Floquet theory as a complement to design-oriented models in order to ensure a robust operation. The approach is applied to a constant frequency V^2 peak control and to $V^2 I_c$ control and it is validated experimentally on a 5 MHz Buck converter with $V^2\,I_c$ control.

By comparing the proposed methodology to the stability criteria of design-oriented models, important conclusions have been obtained that are summarized here.

1) Design-oriented models are very useful but rely on simplifications such as assuming a negligible influence of the ESL of the output capacitor or a perfect sensing of signals. These simplifications limit their accuracy and it is important to study under which cases the simplifications are valid.
2) In ripple-based controls, design-oriented models neglect the influence of the slow loop in the stability but, in fact, even a low-bandwidth linear controller can critically affect the stability of the converter. The paper shows a case for a constant frequency V^2 peak control where the minimum switching frequency to assure stability with the slow loop open is 300 kHz and, when the slow loop is closed with a bandwidth of $f_{sw}/40$, the minimum switching frequency is increased to 400 kHz.
3) When precise regulation of the output voltage is not required and therefore the slow loop is not included in the control, the design-oriented stability criterion for the constant frequency V^2 peak control is only valid when the size of the output capacitor is high and overcompensates the designs when the size of the output capacitor is low. The paper shows a case for $C = 50\,\mu$ F where the design-oriented stability criterion forces the designer to operate at a minimum switching frequency of 330 kHz when, in reality, the converter is stable from 230 kHz.
4) Design-oriented models can be used to define an initial design but a more accurate analysis is needed to refine, if required, the initial design to a final robust design.

APPENDIX A

PIECE-WISE MODEL OF $V^2 I_c$

This appendix contains the detailed expression of the piece-wise model of $V^2 I_c$. The piece-wise smooth model of the system (see Fig. 10) is

$$\frac{dx(t)}{dt} = \begin{cases} A_0 x(t) + B_0 u, & \text{if state is 0} \\ A_1 x(t) + B_1 u, & \text{if state is 1} \end{cases} \tag{33}$$

where

$$x(t) = \left(v_c(t), v_s(t), i_L(t), i_c(t), i_s(t) v_f(t)\right)^T \tag{34}$$

$$u = (V_{\text{in}}, V_{\text{ref}}, I_{\text{load}})^T; \quad K_i = 1/(R_f C_f) \tag{35}$$

$$A_0 = \begin{pmatrix} 0 & 0 & 0 \\ 0 & 0 & 0 \\ 0 & 0 & \dfrac{-(R_0 + R_L + R)}{L} \\ -1/\text{ESL} & 0 & R/\text{ESL} \\ 0 & -1/L_S & R/L_S \\ 0 & 0 & -K_i K_{vs} R \end{pmatrix} \begin{pmatrix} 1/C & 0 & 0 \\ 0 & 1/C_S & 0 \\ R/L & R/L & 0 \\ -(R + \text{ESR})/\text{ESL} & -R/\text{ESL} & 0 \\ -R/L_S & -(R + R_S)/L_S & 0 \\ K_i K_{vs} R & K_i K_{vs} R & 0 \end{pmatrix} \tag{36}$$

$$A_1 = \begin{pmatrix} 0 & 0 & 0 \\ 0 & 0 & 0 \\ 0 & 0 & -\dfrac{(R_1 + R_L + R)}{L} \\ -1/\text{ESL} & 0 & R/\text{ESL} \\ 0 & -1/L_S & R/L_S \\ 0 & 0 & -K_i K_{vs} R \end{pmatrix} \begin{pmatrix} 1/C & 0 & 0 \\ 0 & 1/C_S & 0 \\ R/L & R/L & 0 \\ -(R + \text{ESR})/\text{ESL} & -R/\text{ESL} & 0 \\ -R/L_S & -(R + R_S)/L_S & 0 \\ K_i K_{vs} R & K_i K_{vs} R & 0 \end{pmatrix} \tag{37}$$

$$B_0 = \begin{pmatrix} 0 & 0 & 0 \\ 0 & 0 & 0 \\ 0 & 0 & R/L \\ 0 & 0 & -R/\text{ESL} \\ 0 & 0 & -R/L_S \\ 0 & K_i & K_i K_{vs} R \end{pmatrix}; B_1 = \begin{pmatrix} 0 & 0 & 0 \\ 0 & 0 & 0 \\ 1/L & 0 & R/L \\ 0 & 0 & -R/\text{ESL} \\ 0 & 0 & -R/L_S \\ 0 & K_i & K_i K_{vs} R \end{pmatrix} \tag{38}$$

Notice that if the on-resistances of the MOSFET transistors R_1 and R_0 are the same, then, $A_1 = A_0$.

The switching conditions at the first and second event are

$$h_{10}(x, t) = Kx(t) + Gu + m_{\text{ramp}} t + H \tag{39}$$

$$h_{01}(t) = t - T \tag{40}$$

where

$$K = (0, 0, K_v R, -K_v R, nK_{ic} - K_v R, -1) \tag{41}$$

$$G = (0, -1, -K_v R). \tag{42}$$

Notice that the second switching event is forced by the latch RS to provide a constant switching frequency and, thus, it does not depend on the state variables.

APPENDIX B

FLOQUET THEORY APPLIED TO POWER CONVERTER

The Floquet theory addresses the problem of determining the stability of periodic systems. The theory states that the periodicity of a periodic system can be maintained if the eigenvalues, called the Floquet multipliers, of the monodromy matrix, ϕ_{cycle}, are all inside the unit circle. The monodromy matrix is the matrix that relates the perturbation at the beginning of a period and the perturbation at the end of that period $\triangle x(T) = \phi_{\text{cycle}} \cdot \triangle x(0)$. Consequently, the Floquet theory establishes whether a perturbation will grow or not over a period.

Depending on the system, several methods to compute the monodromy matrix are available. Periodic systems can be classified in three types: continuous systems, discrete systems, and hybrid systems.

A. Monodromy Matrix of Discrete Systems

A discrete system [18] is of the form of $x_{k+1} = f(x_k, u)$, where x_k is the state at the beginning of the period, x_{k+1} is the state at the end of the period, u is the input variables, and f is, in general, a nonlinear function. The monodromy matrix of discrete systems is equal to the Jacobian of the discrete system evaluated in a period

$$\phi_{\text{cycle}}(x_k, u) = \frac{\partial f(x_k, u)}{\partial x_k}. \tag{43}$$

B. Monodromy Matrix of Hybrid Systems

A hybrid system is a system that presents both continuous and discrete transitions. An example of such system is a piece-wise smooth system that is of the form of

$$\frac{dx(t)}{dt} = \begin{cases} A_0 x(t) + B_0 u, & \text{if state 0} \\ \cdots & \\ A_n x(t) + B_n u, & \text{if state n.} \end{cases} \tag{44}$$

A model of this form can be easily derived for a power converter.

The monodromy matrix of hybrid systems is constructed by premultiplying transition matrices and saltation matrices [17]. Each of them takes into account the evolution of the perturbation during different times of the period:

1) The transition matrix is the matrix that evaluates the evolution of a perturbation in a continuous system. In case the system evolves from $t = 0$ to $t = dT$ in state i ($dx(t)/dt = A_i x(t) + B_i u$), then the transition matrix is $\phi_i(dT) = e^{A_i dT}$.
2) The saltation matrix [17], [19] is the matrix that evaluates the evolution of the perturbation across a switching hyper-surface. The switching surface is defined with the zero-level set function $h(x, t)$ that, in power converters, is commonly of the form

$$h(x(t), t) = Kx(t) + Gu + m(t) \tag{45}$$

where the condition to commutate the switches depends on the state variables,$x(t)$, the input, u, and an external time-varying signal, $m(t)$, which can be for example a ramp.
The saltation matrix, S, [19] is obtained from the formula

$$S = I + \frac{(f_{p+} - f_{p-})n^T}{n^T f_{p-} + \frac{\partial h}{\partial t}(t_p, x(t_p))} \tag{46}$$

where I is the identity matrix, f_{p-} is the differential state dx/dt just before the switching, f_{p+} is the differential state dx/dt just after the switching, n is the normal to the hyper-surface $h(x(t), t)$ ($n = K$ if (45) applies), and t_p is the instant of the period at which the system commutates.

Notice that when the switching is forced (as in controls using a latch RS), the switching condition is not an actual hyper-surface[3] and, therefore, the term n of the equation (46) is a vector of zeros. Consequently, the saltation matrix at that instant is the identity matrix.

To build the monodromy matrix, the "path" traveled by the perturbation needs to be followed. For a system that starts in state 1, then at $t = t_1$, it switches to state 0 and continues in that state until it switches back at $t = t_2$ to state 1, the monodromy matrix is

$$\phi_{\text{cycle}} = S_0(t_2) \cdot e^{A_0 \cdot (t_2 - t_1)} \cdot S_1(t_1) \cdot e^{A_1 \cdot t_1}. \tag{47}$$

This expression takes into account the overall evolution of the perturbation. The evolution during state 1 is the transition matrix $e^{A_1 \cdot (t_1)}$, the evolution across the first switching is the saltation matrix $S_1(t_1)$, the evolution during state 0 is the transition matrix $e^{A_0 \cdot (t_2 - t_1)}$ and the evolution across the second switching is the saltation matrix $S_0(t_2)$.

REFERENCES

[1] M. Del Viejo, P. Alou, J. Oliver, O. Garcia, and J. Cobos, "V2ic control: A novel control technique with very fast response under load and voltage steps," in *Proc. IEEE 26th Annu. Appl. Power Electron. Conf. Expo.*, 2011, pp. 231–237.

[2] Y. Yian, P.-H. Liu, F. Lee, Q. Li, and S. Tian, "V2 control with capacitor current ramp compensation using lossless capacitor current sensing," in *Proc. IEEE Energy Convers. Congr. Expo.*, 2013, pp. 117–124.

[3] S. Huerta, P. Alou, J. Oliver, O. Garcia, J. Cobos, and A. Abou-Alfotouh, "Design methodology of a non-invasive sensor to measure the current of the output capacitor for a very fast non-linear control," in *Proc. IEEE 24th Annu. Appl. Power Electron. Conf. Expo.*, 2009, pp. 806–811.

[3] An hyper-surface must depend on the state variables and be differentiable with respect to them. In the case of a forced switching, the switching condition is time-dependent only and, therefore, $S = I$.

[4] S. Huerta, A. Soto, P. Alou, J. Oliver, O. Garcia, and J. Cobos, "Advanced control for very fast dc–dc converters based on hysteresis of the cout current," *IEEE Trans. Circuits Syst. I: Regular Papers*, vol. 60, no. 4, pp. 1052–1061, Apr. 2013.

[5] F. Tan and R. Middlebrook, "A unified model for current-programmed converters," *IEEE Trans. Power Electron.*, vol. 10, no. 4, pp. 397–408, Jul. 1995.

[6] W. Tang, F. Lee, and R. Ridley, "Small-signal modeling of average current-mode control," *IEEE Trans. Power Electron.*, vol. 8, no. 2, pp. 112–119, Apr. 1993.

[7] J. Li and F. Lee, "Modeling of v^2 current-mode control," *IEEE Trans. Circuits Syst. I: Reg. Papers*, vol. 57, no. 9, pp. 2552–2563, Sep. 2010.

[8] S. Tian, K.-Y. Cheng, F. Lee, and P. Mattavelli, "Small-signal model analysis and design of constant-on-time v2 control for low-esr caps with external ramp compensation," in *Proc. IEEE Energy Convers. Congr. Expo.*, 2011, pp. 2944–2951.

[9] S. Tian, F. C. Lee, P. Mattavelli, and Y. Yan, "Small-signal analysis and design of constant frequency v2 peak control," in *Proc. IEEE 28th Annu. Appl. Power Electron. Conf. Expo.*, 2013, pp. 1717–1724.

[10] Y. Yan, F. C. Lee, P. Mattavelli, and S. Tian, "Small signal analysis of v2 control using current mode equivalent circuit model," in *Proc. IEEE 28th Annu. Appl. Power Electron. Conf. Expo.*, 2013, pp. 1709–1716.

[11] Y. Yan, F. Lee, and P. Mattavelli, "Unified three-terminal switch model for current mode controls," *IEEE Trans. Power Electron.*, vol. 27, no. 9, pp. 4060–4070, Sep. 2012.

[12] D. Giaouris, S. Maity, S. Banerjee, V. Pickert, and B. Zahawi, "Application of Filippov method for the analysis of subharmonic instability in dc–dc converters," *Int. J. Circuit Theory Appl.*, vol. 37, no. 8, pp. 899–919, 2009.

[13] A. El-Aroudi, B. Robert, and L. Martínez-Salamero, "Modelling and analysis of multicell converters using discrete time models," in *Proc. IEEE Int. Symp. Circuits Syst.*, 2006, pp. 4–2164.

[14] R. Redl and J. Sun, "Ripple-based control of switching regulators—An overview," *IEEE Trans. Power Electron.*, vol. 24, no. 12, pp. 2669–2680, Dec. 2009.

[15] A. El-Aroudi, J. Pelaez, M. Feki, and B. G. M. Robert, "Stability analysis of two-cell buck converter driven dc motor with a discrete-time closed loop," in *Proc. 6th Int. Multi-Conf. Syst., Signals Devices*, 2009, pp. 1–6.

[16] H. R. Visser and P. P. J. Van den Bosch, "Modelling of periodically switching networks," in *Proc. IEEE 22nd Annu. Power Electron. Spec. Conf.*, 1991, pp. 67–73.

[17] A. Filippov, *Differential Equations with Discontinuous Righthand Sides: Control Systems (Mathematics and its Applications)*. New York, NY, USA: Springer-Verlag, 1988.

[18] M. di Bernardo and F. Vasca, "Discrete-time maps for the analysis of bifurcations and chaos in dc/dc converters," *IEEE Trans. Circuits Syst. I: Fund. Theory Appl.*, vol. 47, no. 2, pp. 130–143, Feb. 2000.

[19] R. I. Leine and H. Nijmeijer, *Dynamics and Bifurcations of Non-Smooth Mechanical Systems (Lecture Notes in Applied and Computational Mechanics)*. New York, NY, USA: Springer-Verlag, 2010.